Thermo-mechanical modeling of polymer spur gears with experimental validation using high-speed infrared thermography

Cerne, Borut; Petkovsek, Martin; Duhovnik, Joze; Tavcar, Joze

Published in:
Mechanism and Machine Theory

DOI:
10.1016/j.mechmachtheory.2019.103734

2020

Document Version:
Publisher's PDF, also known as Version of record

Mechanism and Machine Theory 146 (2020) 103734

Contents lists available at ScienceDirect

Mechanism and Machine Theory

journal homepage: www.elsevier.com/locate/mechmachtheory

Research paper

Thermo-mechanical modeling of polymer spur gears with experimental validation using high-speed infrared thermography

B. Černe*, M. Petkovšek, J. Duhovnik, J. Tavčar

Faculty of Mechanical Engineering, University of Ljubljana, Akerčeva 6, 1000 Ljubljana, Slovenia

ARTICLE INFO

Article history:
Received 12 September 2019
Revised 14 November 2019
Accepted 25 November 2019

Keywords:
Polymer gears
Thermal analysis
Sliding friction
Contact mechanics
IR thermography,

ABSTRACT

The presented work is focused on the development of a comprehensive thermo-mechanical model for predicting the temperature rise in thermoplastic polymer spur gears with any desired profile geometry while running. The specific constitutional behavior of thermoplastics influences the gear-meshing pattern, which can deviate substantially from ideal gear meshing, as typically exhibited by metal gears in moderate-loading conditions. Taking this aspect into account is of paramount importance if realistic temperature-rise predictions are to be made. The thermal response of the considered gear pair is studied thoroughly from both the analytical and experimental standpoints. Good agreement was found between the results of the model and the experimental measurements performed using a high-speed thermal imaging infrared camera, although it was also observed that the real-life temperature rise can increase noticeably if large geometric tolerance deviations from the ideal profile geometry are present. The presented experimental approach also offers the possibility to observe the temperature rise inside and outside the meshing cycle.

1. Introduction

Polymer gears are exposed to continuous cyclic loading conditions where, due to the frictional and structural losses, the temperature in the gear structure can rise to levels that can have a noticeable impact on their durability and life expectancy. Focusing specifically on cylindrical polymer gears, their design nowadays relies primarily on existing standards and guidelines, of which currently the most complete and likely the most widely used is the VDI2736 [1,2] guideline. The two most relevant parameters in assessing the load-carrying capacity of polymer gears are the root and flank fatigue strength, which, for polymer gears, are both defined as a function of the temperature. It is, therefore, very important to possess a reliable tool for the prediction of the temperature rise during gear running in order to properly design a high-performance polymer gear pair.

The VDI 2736 guideline also provides a simplified model for the evaluation of the flank and root temperature rise based on the empirical Hachmann-Strickle model [3]. While the model is, due to its simplicity, handy for quick estimations of the

* Corresponding author.
E-mail addresses: borut.cerne@fs.uni-lj.si, borut.cerne@lecad.fs.uni-lj.si (B. Černe).
URL: http://www.fs.uni-lj.si/en/ (B. Černe)

https://doi.org/10.1016/j.mechmachtheory.2019.103734

Nomenclature

Symbols:

α	Thermal diffusivity
α_{p}	Pressure angle
β	Hysteresis loss coefficient
χ	Plasticity index
δ_{ij}	Kronecker delta tensor
η	Dynamic viscosity
λ	Kinematic viscosity
μ	Coefficient of friction
ν	Poisson's ratio
ω	Angular velocity
ψ	Partitioning coefficient
ρ	Density
σ	Stress
σ'	Hydrostatic stress
τ	Shear stress
A	Area
b	Gear face width
c	Contact interface half-width
c_{p}	Specific heat
d	(Pitch circle) diameter
E_{c}	Characteristic elastic modulus
F_{n}	Normal contact force
F_{t}	Tangential force
H_{m}	Microhardness
H	Heaviside function
h	Convective heat-transfer/conductance coefficient
i	Transmission ratio
k	Thermal conductivity
l	Path length/active tooth profile length
L	Tooth thickness
n	Running speed
Nu	Nusselt number
p	Pressure
P	Hermite polynomial
Pr	Prandtl number
q	Heat flux
R	Radius
Re	Reynolds number
s	Tooth-profile domain coordinate
t	Time
$\tan(\theta_{\mathrm{c}})$	Root-mean-square asperity slope angle
T	Temperature
v_{s}	Sliding speed
W	Energy
Z_{ε}	Contact ratio factor
Z_{E}	Elasticity factor
Z_{H}	Zone factor

Indices

1	Driver gear
2	Follower gear
a	Gear tip
b	Gear base
c	Contact domain
d	Running cycle
f	Flash component

m	Mean
n	Nominal component
r	Rolling
s	Shear
t	Tangential
u	Meshing cycle
z	Number of gear teeth

temperature rise, it can, as noted by Beermann in [4] and Pogačnik et al. in [5], in many instances lead to unrealistic results. Several attempts have been made to construct better temperature models, which in most cases rely on numerical computational methods and are more in line with the physical nature of the process. Basically, all existing temperature models for gears and, in fact, for most cyclically loaded engineering systems, follow a temperature-superposition approach, where the overall temperature rise is the sum of the so-called nominal (or bulk) temperature and flash-temperature rises (see e.g. the work by Kennedy et al. [6]). The first typically denotes the long-term temperature rise throughout the gear structure, while the second defines the local, almost instantaneous, temperature rise around the area where the heat losses are generated. The flash-temperature component, as defined in the Blok model [7], was applied for the case of gear meshing and was also considered, e.g., in the work of Mao in [8]. In the latter, a numerical model for the prediction of the flash-temperature rise during an entire meshing cycle was presented. It was confirmed that the Blok model could be used to evaluate the average flash-temperature rise, while the numerical solution offers a more holistic insight into flash-temperature variations during the meshing. The Takanashi model, presented in [9] and also described by Erhard in [10], offers an analytical solution for the evaluation of the nominal temperature rise due to frictional and viscoelastic deformation losses. Luo et al. [11] presented a finite-element method (FEM) thermal model for the nominal temperature prediction of lubricated metal gears based on theoretical predictions of the contact-pressure distribution and sliding speed during meshing. Fernandes et al. [12] provide a comprehensive numerical approach using a FEM for the evaluation of the bulk- and flash-temperature components. In their model the frictional heat losses driving the temperature rise are calculated based on the power-loss approach described by Marques et al. in [13].

An advanced approach for the thermo-mechanical modeling of thermoplastic spur gears is presented also by Doll in [14]. Especially notable is the consideration of the viscoelastic response of the studied polymer (PEEK) to dynamic loading conditions in a wide range of load frequencies and temperatures using DMA (dynamic mechanical analysis). Also, the author presents experimental findings regarding the coefficient of friction as a function of temperature, speed and contact pressure. In our earlier investigation [15] we presented a method for the evaluation of heat losses using a transient mechanical FEM analysis, through which we could evaluate the contact response (i.e., the contact pressure, contact area and sliding speed) and the resulting frictional heat flux, which predominantly drives the temperature rise. The method enables the consideration of any type of gearing geometry and also the influence of any variations in the geometry, like profile modifications or even tolerance deviations [16]. In our more recent study [17] a flash-temperature model is developed based on the just-described approach that enables an efficient evaluation of the time-dependent flash-temperature pattern during the gear meshing and also provided a basic component of the analysis approach presented here. A similar approach was also considered in a recent study by Roda-Casanova et al. [18].

A key point in providing a strong foundation for any developed model is a thorough experimental validation of the model results. In the studied system this can be done by comparing the evaluated temperature results with temperature measurements performed using different tools. The most typical measurement approach in recent years has been the use of infrared (IR) cameras, e.g., in [5,19–21]. Common to all these reports is the use of IR cameras with too low frame rates and integration times for an accurate visualization of the gear-tooth temperature field during running. This type of measurement equipment can suffice for a comparative analysis of the thermal performance of different gear pairs, but is inadequate for absolute temperature measurements at any given point on the gear's outer surfaces, let alone for a measurement of the local contact-temperature rise. One exception is the report by Letzelter et al. [22], where a high-speed camera is employed for an experimental study of the temperature rise in PA66 spur gears. The camera is calibrated by determining the emissivity factor of the chosen material, which was found to be a very high value of 0.99. The authors also point out the problems when attempting to measure the local contact temperature due to surrounding airflow turbulence and decreased emissivity when the angle of the camera to the surface is less than 45°. The IR camera employed in their study, however, still has a relatively low frame rate, which enables relatively clear measurements only at lower running speeds.

While many contributions have been added, especially in the last couple of years, to the field of polymer-gear thermal analysis, we still see several discrepancies in the current approaches, both analytical and experimental, that need to be addressed. First of all, based on findings in the literature and also our own research, we do not regard analytical models like the Hachmann-Strickle or the Takanashi model to be able to fully account for all the factors influencing the magnitude of the temperature rise, which means they have rather limited applicability. The existing numerical models provide a much more reliable and physically consistent tool for the temperature evaluation (we point out here especially the models by Fernandes et al. [12] and Doll [14], which to the best of our knowledge are currently two of the most consistent available models), even though we still see many potential upgrades that could lead to even more accurate results. Furthermore, the majority

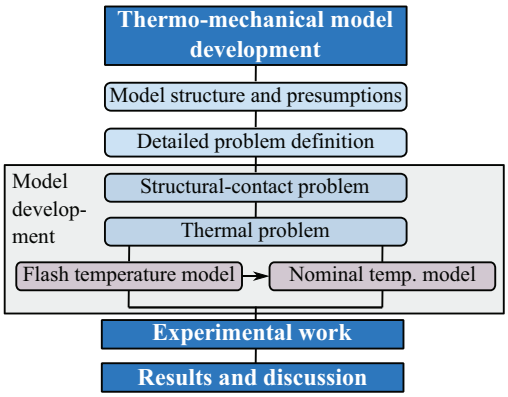

Fig. 1. Summary of this paper's content.

of these models is limited to involute gear profiles, two exceptions being the models by Roda-Casanova et al. [18] and Doll [14].

In our investigation we attempt to improve on the existing thermal analysis methods for polymer spur gears in several ways. First of all we base the evaluation of the sliding-friction heat losses on transient mechanical FEM analyses, which provide the most accurate way of calculating these losses as a function of time and location for any desired gearing geometry (i.e., not only for involute gears) and materials (the stiffness and related mechanical properties of the materials also play a major role in the gear meshing kinematics). The analysis geometry considered in our evaluations is correlated as accurately as possible to the geometry of the experimental test samples by using a high-accuracy 3D scanning technology in order to ensure that we considered comparable geometric conditions in our validation process. Furthermore, we show that a key feature in a consistent thermal analysis is the inclusion of associated components, like the shaft, fasteners, etc., which can influence noticeably the heat-dissipation process. Additionally, we present a set of physically consistent models for a correct evaluation of the convective heat-transfer coefficients, based on the specific types of surface geometries, which again have a decisive importance in correctly determining the temperature rise. With the presented approach we wish to prove that in a practically applicable range of running conditions and running time frames, fairly accurate temperature predictions can be made, even when employing mostly linear system assumptions. A key part of our research is also the experimental validation procedure, carried out using a high-speed IR camera that enabled very accurate measurements of the temperature gradient on any single gear tooth during running, which offered us the chance to assess in detail the correlation between the developed model and reality. For an easier orientation, we schematically outline the work described in the ensuing pages, as shown in Fig. 1.

2. Thermo-mechanical model development

2.1. Basic model structure and underlying presumptions

The thermo-mechanical model presented in the following is constructed in a sequential configuration, where we initially perform a detailed structural-contact analysis using a FEM, based on which a thermal analysis for the evaluation of the overall temperature rise during gear running can be performed. A typical approach when dealing with the thermal analyses of cyclically loaded systems is, as already mentioned, to consider the overall temperature increase as a superposition of two components, i.e., the flash-temperature rise and the nominal (or bulk) temperature rise, or

$$\Delta T = \Delta T_{\mathrm{f}} + \Delta T_{\mathrm{n}}. \tag{1}$$

The flash-temperature rise is considered as being the local (almost) instantaneous temperature increase at the thermal loading point, which is in this case the tooth pair contact interface and is a consequence of the sliding (and in some small part rolling) frictional losses. The nominal temperature rise is, on the other hand, the long-term rise due to the heat accumulated after a larger number of running/loading cycles.

The analyzed polymer-gear system can, due to the complex thermo-mechanical nature of the considered thermoplastics, in some instances (e.g., if a high torque load is applied) be rather nonlinear in its phenomenological behavior and, hence, very troublesome to model correctly. However, in order to keep the model in a manageable and realistically usable form, while still providing adequate consistency with the real-life behavior of the system, the following set of presumptions needs to be considered:

(i) The generated heat losses are predominantly a consequence of sliding friction.
(ii) The coefficient of friction (COF) is independent of the temperature, sliding speed and contact stress.

Table 1
Thermo-mechanical parameters of the considered materials.

Parameter	Symbol [Unit]	POM	PA66
Density	ρ[kg/m3]	1410	1150
Elastic modulus [23]	E [MPa]	2800	3500
Tensile yield strength	R_m [MPa]	67	84
Elongation at yield	ε_y [/]	0.09	0.07
Poisson's ratio	ν [/]	0.35	0.4
Specific heat	c_p [J/(kgK)]	1400	1500
Thermal conductivity	k [W/(mK)]	0.39	0.36
COF [2]	μ[/]	0.18 (dry running)	

Table 2
Geometry parameters of the gear pair.

Parameter	Symbol [unit]	Value
Transmission	i [/]	1
Module	m [mm]	1
Number of teeth	z [/]	20
Pressure angle	α_p [°]	20
Gear width	b [mm]	6
Gear-hub diameter	d_h [mm]	6
Tooth thick. tol. [25]	e25 [µm]	$-30/-60$
Tip rounding	r_t [mm]	0.03

(iii) The generated heat losses are released entirely through the contact surfaces and distributed between the contacting bodies in a specific ratio.
(iv) The heat losses are distributed across a theoretical contact area
(v) The gear-meshing kinematics remain consistent throughout the gear-pair running period.
(vi) The thermal and mechanical material properties can, in the considered range of the temperature increase, be regarded as independent of the temperature.
(vii) The considered materials can be modeled as linearly elastic.
(viii) The temperature rise is independent of the radiation heat dissipation, but dependent on the convection and structural heat dissipation.
(ix) The gear pair is exposed to low or moderate loading conditions, where the system can still reach a (quasi)steady thermal state.
(x) The gears are not run for extended time periods.

The most salient points regarding the presumptions noted above are elaborated in more detail in the Results and discussion section.

2.2. Detailed problem definition

For the development of our model a specific polymer involute spur gear pair case is considered that is in line with the test sample geometries and materials used on the available experimental gear-testing equipment. This will enable a direct validation of the model's results with the experimental measurements.

2.2.1. Material combination

A gear pair composed of two thermoplastic materials will be considered, i.e., polyoxymethylene (POM) for the driver gear and polyamide 66 (PA66) for the follower gear. Specifically, the thermo-mechanical parameters for two specific material grades will be considered, based on test samples from our experimental tests, i.e., Ensinger Tecaform AH natural (POM) and Ensinger Tecamid 66 natural (PA66). Both material grades are available as semi-finished products in rod form, from which the gears can be cut. The main thermo-mechanical properties of the materials are presented in Table 1.

2.2.2. Gear-pair geometry

The main parameters of the gear-pair geometry used for our experimental test samples and also as our case study for the model development are presented in Table 2. A pair of gears with the same number of teeth and hence a transmission ratio of $i = 1$ is used for our tests. The tooth geometry is produced based on the ISO 53 [24] standard using a rack profile A. In accordance with the sample-production parameters we also need to consider the chosen gear backlash (according to the standard DIN 3967 [25]) and tip rounding. The achievable quality of the produced gears is in class Q10 according to the ISO 1328 [26] standard.

A common issue with thermoplastics is dimensional instability, which is especially pronounced in components produced with injection molding, and to a somewhat lesser degree also in machined components. Furthermore, the specific geometric

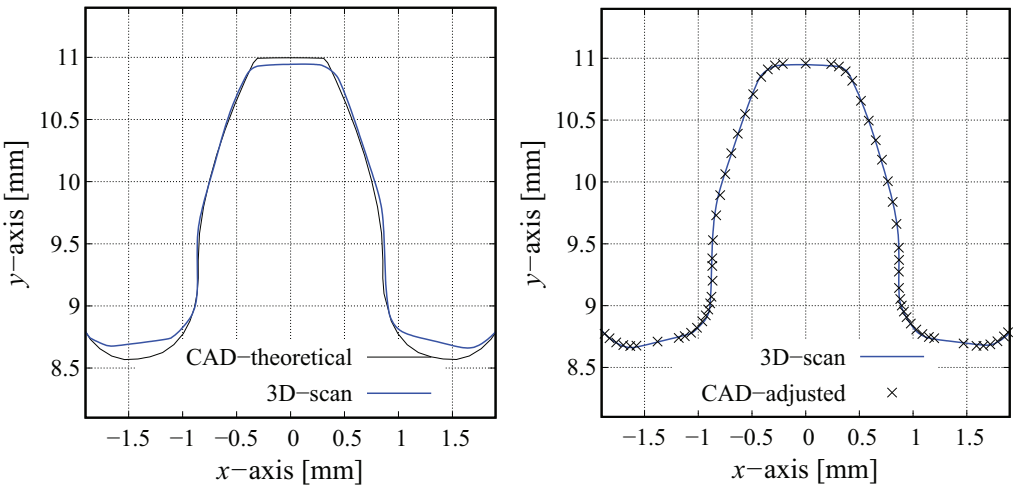

(a) Theoretical vs. measured (b) Correction of the CAD model

Fig. 2. A comparison between the theoretical (CAD) and the measured (3D scan) gear-profile geometry, and the adjustment of the CAD geometry based on measurements.

Table 3
Load cases considered for the flash-temperature evaluation.

	Torque [Nm]	Rot. speed [min^{-1}]
1.)	0.4	956
2.)	0.6	1147
3.)	0.8	1434

requirements of the machining tool (i.e., edge roundings, etc.) can influence the final geometry of the gears. It is, therefore, recommended to perform detailed measurements of the tooth geometry of the produced gears in order to be sure of all the parameters and also to be able to recreate as accurately as possible the used gear geometry in our model. For our measurements a high-precision 3D scanner ATOS Compact Scan 5M was used (scan accuracy 0.002μm in the used scan window). A comparison of the theoretical CAD tooth profile geometry (with mean tolerance values), created using KissSoft software, and the 3D scanned profile (taken at the middle of the tooth-face width) is shown in Fig. 2.

The method (gear cutting from rods) produced noticeable deviations from the initially designed solution. The average deviation of the measured root diameter relative to the mean theoretical value was 0.257mm, while the tip diameter, tip-rounding radius and the tooth thickness diverged, on average, by 0.1 mm, 0.225 mm and 0.03 mm, respectively. Furthermore, the root rounding was found to be elliptical instead of cylindrical, as was prescribed in the theoretical model. These kinds of deviations can have a major influence on the contact response and the root stresses during gear meshing and, consequently, on the frictional thermal losses. In our further analyses the modified CAD geometry based on the 3D scans presented in Fig. 2b will be considered.

2.2.3. Running conditions

The model was applied to, and experimentally validated for, several different running conditions. The considered running load parameters are noted in Table 3. The evaluations and experimental tests were performed at all nine possible torque/running-speed combinations.

2.3. Structural contact problem

The first part of our model procedure involves a detailed structural contact analysis simulating an entire gear-meshing cycle using a FEM. This type of time-dependent analysis involves large deflections and the application of frictional contacts, both turning the problem into a nonlinear one. In our case we employed ANSYS Workbench FEM software to perform the analysis. The geometric features of the spur gears enable a reduction of the problem to a 2D plane-stress case. The constructed boundary conditions and finite-element (FE) mesh are presented in Fig. 3. The key analysis parameters of the developed FE model are shown in Table 4.

To obtain consistent contact-response results from the analysis it is important to have the correct choice of two contact settings, i.e., the penetration tolerance and the radius of the contact identification (referred to as the “Pinball region” in ANSYS). For the Pinball region we, in general, want to use as low a value as possible, while the penetration tolerance needs to be chosen more carefully, as it can quickly lead to unrealistic escalations of the contact stresses. A good method to

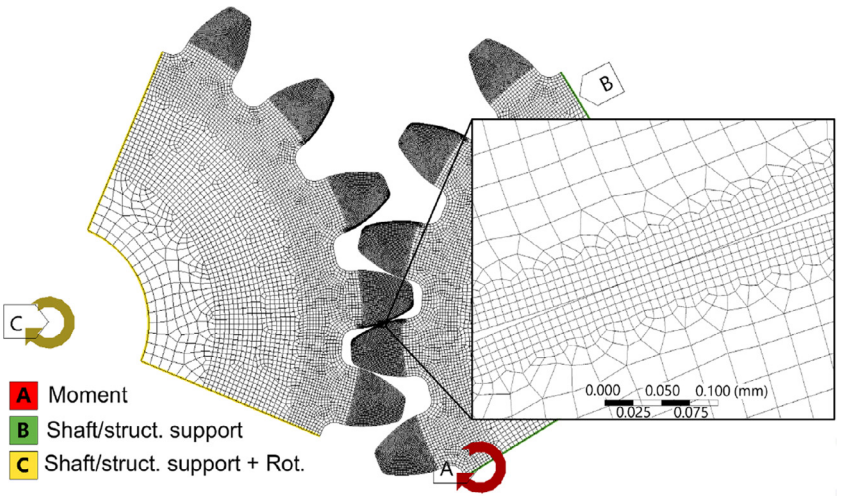

Fig. 3. Constructed FE mesh and applied boundary conditions.

Table 4
FE mesh parameters.

Model parameter	Type/Value
Structural FE [27]	PLANE183
Contact FE [28]	CONTA172/TARGE169
FE size	0.3mm-0.0075 mm
Shape fun. approx. order	Quadratic
Elem. quality (min./max./mean.) [29]	0.36/1.0/0.97
Number of FE nodes KE	126e3
Number of time steps	> 280
Contact type	Frictional contact
Coefficient of friction	0.18 [2]
Contact formulation	Augmented Lagrange
Contact behavior	Symmetric
Penetration tolerance	0.0019 mm
Radius of contact identification	0.011 mm

identify the correct parameters is to compare the numerically evaluated contact pressure at the pitch point with the results obtainable from Hertzian theory for a two-cylinder contact, as presented in [30] or the adapted evaluation method for gears, as presented in the guideline VDI 2736 [2]. Based on the latter, the theoretical maximum contact pressure can be identified using the equation

$$p_c = Z_E \cdot Z_H \cdot Z_\varepsilon \cdot \sqrt{\frac{F_t}{b \cdot d_1} \cdot \frac{i+1}{i}}. \tag{2}$$

Here Z_E is the elasticity factor, Z_ε is the contact ratio coefficient, while Z_H is the so called zone factor that takes into account the tooth profile curvature at the pitch point and the conversion from tangential (F_t) to normal (F_n) contact force. The peak contact-pressure response evaluated using the FEM normally coincides very well with the results using Eq. (2) if the correct contact parameters are set (deviations do not exceed 2%).

The FEM analysis of the contact response on both gears is performed for the middle tooth pair, as shown in Fig. 3. The analysis was performed on an HPC cluster using the intrinsic MPI parallel processing platform. Good scalability of the model was, however, obtainable only up to 32 CPU cores.

Using the software post-processor the time-dependent peak contact-pressure results and contact area, which are necessary for the subsequent thermal analysis, are directly obtainable. An additional variable, which is essential for the thermal analysis, but cannot be directly obtained from the software post-processor, is the sliding speed. In order to evaluate this variable we need to decouple the sliding and rotational components from the overall movement of the contact interface during gear meshing. A method for the evaluation of the sliding speed, based on a structural-contact FE analysis as presented here, is described in our previous paper [17]. Typical contact-analysis results, considering the geometric, material and FE mesh properties described in the previous pages, are presented in Fig. 4 (load conditions: $n = 1147\ \text{min}^{-1}$ and $M = 0.8\,\text{Nm}$).

Here, the points A and E mark the beginning and the end of the meshing cycle, B and D are the points of initiation and termination of the single tooth contact, while C is the pitch point contact instant. Additionally, it is important to check whether the peak strains, present at the tooth flanks and roots, are in allowable ranges. We noted in Table 1 that the

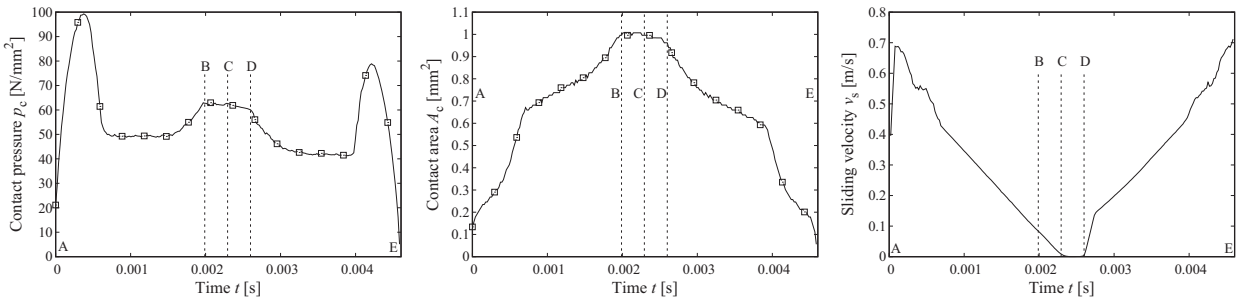

(a) Contact pressure **(b)** Contact area **(c)** Sliding speed

Fig. 4. Contact response results from the described structural contact FEM analysis ($n = 1147$ min^{-1} and $M = 0.8$ Nm).

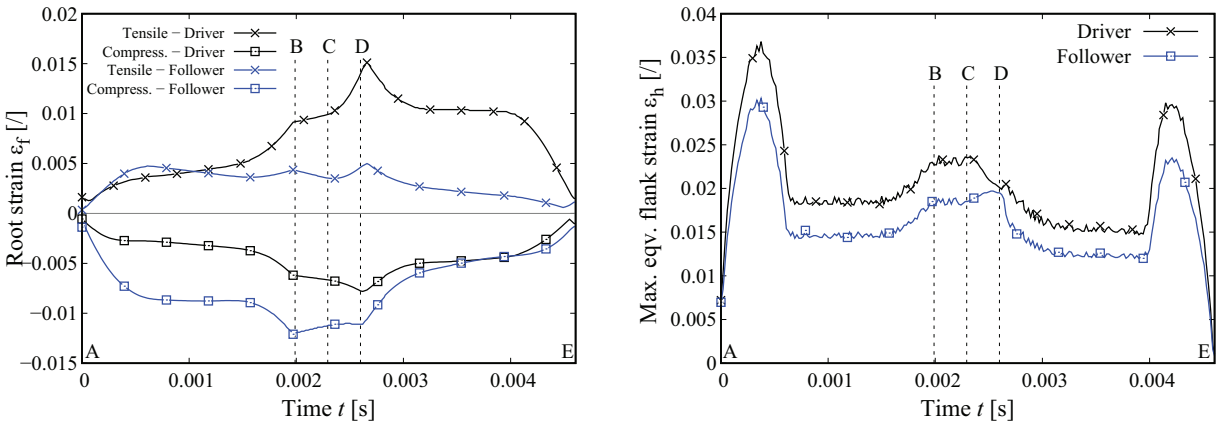

(a) Root bending strains **(b)** Max. eqv. flank strains

Fig. 5. Time-dependent root and flank strains present during the analyzed gear-meshing cycle ($n = 1147$ min^{-1} and $M = 0.8$ Nm).

yield deformations for the considered materials are 9% and 7% for POM and PA66, respectively. The strain patterns present during the analyzed gear-meshing cycle are presented in Fig. 5. The root strains are taken as the normal bending strains in the gear's radial direction, while the flank strains are represented using the peak equivalent von Mises strain format. The evaluated strains are nowhere near the yield points of the chosen materials, for which we can consider the presumption of linear elastic behavior as being adequate from this stand point.

2.4. Thermal problem

The thermal part of the model can now be constructed based on the results from the just described mechanical analysis, as a superposition of two components, i.e., the flash and nominal temperature rise. Both components are a consequence of the same underlying physical processes, the main difference between them being the time window of the manifestation. While the flash temperature is an almost instantaneous temperature rise, occurring separately during each meshing cycle, the nominal temperature rise describes the long-term heat retention in the teeth and gear-body structure and the consequent temperature gradient.

2.4.1. Semi-analytical flash-temperature model

The flash temperature component is rather intricate to model correctly, as it is a transient thermal process. This component was thoroughly studied in our previous paper [17]. Given the very rapid nature of the process and the fact that this temperature rise occurs right under the contact interface, the presumption was made that the heat-dissipation effects, like convective and structural dissipation, do not play a significant role in the resulting temperature rise.

The model developed in the cited work is based on the heat equation, which in this case models the temperature rise on a semi-infinite solid (with $z \leq 0$) due to a moving strip heat source bounded by $-c \leq x \leq c$, $-\infty < y < \infty$ and $z = 0$. The heat source simulates the frictional heat losses at the contact interface. Here, x is the horizontal direction of movement (relative to the body), while y and z are the perpendicular horizontal and vertical coordinates respectively. The coordinate system should be viewed as being attached to the center of the strip contact interface. The latter is modeled as a time- and

space-dependent heat-flux function

$$q_{\mathrm{f}}(x,t) = \mu \cdot v_{\mathrm{s}}(t) \cdot p(x,t) = \mu \cdot v_{\mathrm{s}}(t) \cdot p_{\mathrm{c}}(t) \left[1 - \frac{x^2}{c(t)^2} \right]^{\frac{1}{2}}, \tag{3}$$

where, in accordance with [8,12,31], the contact pressure is modeled as a parabolic function throughout the meshing cycle using Hertzian theory. This presumption was also tested in our mechanical FEM analysis and the results show good agreement between the evaluated contact stress pattern and the parabolic function approximation. The overall frictional heat flux is then partitioned between both contacting bodies based on the presumption of equal temperatures of both bodies at the contact interface, using a time-dependent partitioning coefficient

$$q_{\mathrm{f}}(x,t) = \psi_{\mathrm{f}}(t) \cdot q_{\mathrm{f},1}(x,t) + [1 - \psi_{\mathrm{f}}(t)] \cdot q_{\mathrm{f},2}(x,t). \tag{4}$$

The problem is treated semi-analytically, where the constitutional heat equation is first transformed into integral form using Green's function principle for each separate contacting body (gear). For the meshing tooth on the driver gear we obtain

$$\begin{aligned} \Delta T_{\mathrm{f},1}(x,z,t) = {} & \frac{1}{2\pi\,\rho_1 c_{\mathrm{p}}^1 \alpha_1} \int_0^t \psi_{\mathrm{f}}(t') \int_{-c(t')}^{c(t')} \frac{\mu \cdot v_{\mathrm{s}}(t') \cdot p_{\mathrm{c}}(t')}{t - t'} \\ & \cdot \left[1 - \frac{(x')^2}{c(t')^2} \right]^{\frac{1}{2}} \exp\left\{ - \frac{[(x - x') - v_{\mathrm{s}}(t')(t - t')]^2 + z^2}{4\alpha_1 (t - t')} \right\} \mathrm{d}x' \mathrm{d}t', \end{aligned} \tag{5}$$

or briefly

$$\Delta T_{\mathrm{f},1} = A_1 \int_0^t \psi_{\mathrm{f}}(t') \int_{-c(t')}^{c(t')} f_{\mathrm{f},1}(x',t') \mathrm{d}x' \mathrm{d}t', \tag{6}$$

while for the follower gear tooth we similarly get

$$\Delta T_{\mathrm{f},2} = A_2 \int_0^t [1 - \psi_{\mathrm{f}}(t')] \int_{-c(t')}^{c(t')} f_{\mathrm{f},2}(x',t') \mathrm{d}x' \mathrm{d}t'. \tag{7}$$

Both integrals can be solved numerically using the Gauss quadrature method. By splitting the time- and spatial $x-$ domains into M and N steps, respectively, and using $n_{\mathrm{g}} = 2$ Gauss points per step, we obtain the following solutions

$$\begin{aligned} \Delta T_{\mathrm{f},1}(x_p,t_r) &\approx \textstyle\sum_{j=1}^{M} \psi_j \sum_{i=1}^{N} \underbrace{\sum_{k=1}^{2} \sum_{l=1}^{2} A_1 \frac{t_j - t_{j-1}}{2} \frac{x_i^k - x_{i-1}^k}{2} f_1(x_i^{lk}, t_j^k)}_{F_{ijpr}^1}, \\ \Delta T_{\mathrm{f},2}(x_p,t_r) &\approx \textstyle\sum_{j=1}^{M} (1 - \psi_j) \sum_{i=1}^{N} \underbrace{\sum_{k=1}^{2} \sum_{l=1}^{2} A_2 \frac{t_j - t_{j-1}}{2} \frac{x_i^k - x_{i-1}^k}{2} f_2(x_i^{lk}, t_j^k)}_{F_{ijpr}^2}. \end{aligned} \tag{8}$$

We need to consider that the width of the contact interface surface (in the x direction) is not constant, but changes with time throughout the meshing cycle, hence the x variables in the numerical solution are also time dependent, which complicates the solution. The partitioning coefficient is evaluated for each separate time step t_j using the system of equations

$$\left[\frac{\mathbf{G}_{\mathrm{d}} + \mathbf{G}_{\mathrm{d}}^T}{2} + \frac{\mathbf{G}_{\mathrm{f}} + \mathbf{G}_{\mathrm{f}}^T}{2} \right] \left\{ \bar{\boldsymbol{\psi}} \right\} = \left[\frac{\mathbf{G}_{\mathrm{f}} + \mathbf{G}_{\mathrm{f}}^T}{2} \right] \{ \mathbf{e} \}. \tag{9}$$

where $\mathbf{e}$ is a vector of all ones and

$$\mathbf{G}_{\mathrm{d}} = G_{jr}^{\mathrm{d}} = F_{ijpr}^{\mathrm{d}} e_i e_p \quad \text{and} \quad \mathbf{G}_{\mathrm{f}} = G_{jr}^{\mathrm{f}} = F_{ijpr}^{\mathrm{f}} e_i e_p. \tag{10}$$

Here, e_i and e_p are again vectors of all ones providing a sum for the spatial x-coordinate components. The system constructed in this manner is well-posed and can be solved in a relatively rapid manner using the least-squares singular-value-decomposition method LS-SVD (available, e.g., in the LAPACK library for Fortran or C). The flash-temperature results for the considered case using the described procedure are shown in Fig. 6. The partitioning ratio is almost constant throughout the meshing time at about 0.527. It was observed that the value of the ratio is predominantly dependent on the thermal properties of the contact material pair.

In several other works, like Blok's model [7] and other related models (Luo et al. [11], Fernandes et al. [12]) the partitioning approach returns a non-constant coefficient function. The most likely reason for the discrepancy between these works and ours is that, based on Blok's work, the coefficient is defined as a function of separate contact sliding speed components v_1 and v_2, which typically vary during the meshing cycle. These two component together form the relative sliding speed $v_s = |v_1 - v_2|$, which is evaluated numerically in our approach and used in the partitioning formulation in Eq. (9). In all cases, however, the precondition of equal contact temperature on both contact bodies is fulfilled at every given meshing point.

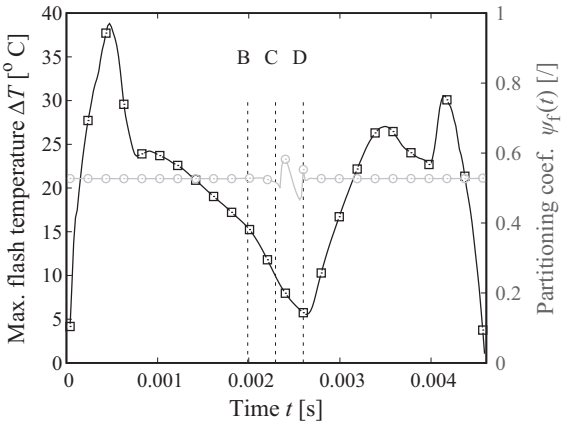

Fig. 6. Flash-temperature results with time-dependent partitioning coefficient $\psi_f(t)$ for the analyzed case.

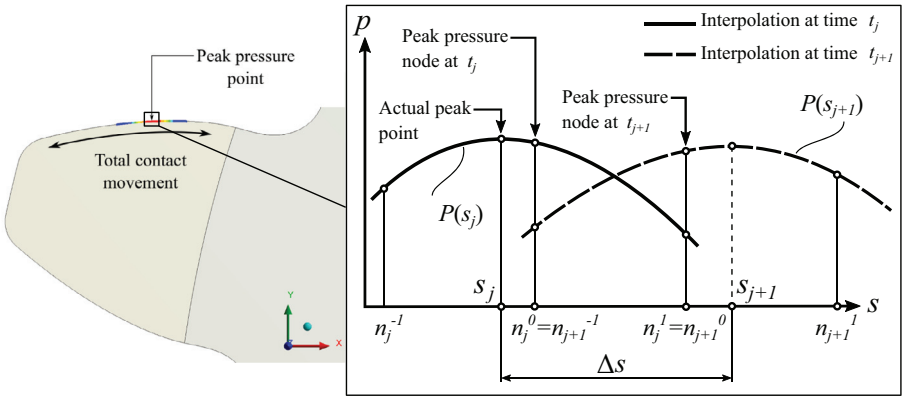

Fig. 7. Evaluation of the total contact movement pattern from the FEM results.

2.4.2. Nominal temperature model using the FEM

The evaluation of the nominal temperature component is slightly more complicated due to the fact that we need to consider several additional factors in the system, like the convective and structural heat dissipations, the influence of the gear geometry, related components, etc. The construction of the model is presented as follows.

Thermal loss function

Perhaps the most challenging part in correctly modeling the nominal temperature rise is the identification of a thermal load function that consistently describes the long-term heat accumulation in the gears. While the flash-temperature rise is a very rapid process by nature, the nominal temperature rise occurs much more slowly (in the range of minutes and hours). To make the numerical analysis of the latter feasible, we need to translate the time-dependent heat-flux function into a time-independent one. To achieve this, we can presume that a constant amount of heat is released during every running cycle at each toot flank, which can simply be evaluated as

$$W_f = \mu \int_0^{t_u} v_s(t) \cdot p_m(t) \cdot A_c(t) \mathrm{d}t, \tag{11}$$

with $p_m(t) = \pi\, p_c(t)/4$ being the mean Hertzian contact pressure at the interface. The released energy is distributed across the active tooth flank based on the movement of the contact interface throughout the meshing cycle. This movement is not dependent solely on the sliding speed, but also on the rolling. This can be defined as the total contact movement (TCM). It can also be evaluated from the FEM analysis results if we fix the coordinate system of observation to the rotating gear (hence viewing the gear as static) and following the peak-pressure point of the contact interface as it moves on the tooth profile during meshing [15]. By identifying the peak-pressure node and the adjacent nodes around it at each time point, and interpolating a Hermite polynomial function $P(s)$ through these nodes, it is possible to identify the (almost) exact location of the peak contact pressure as the zero derivative of the polynomial (see Fig. 7). Following the contact path evaluated in this manner yields a movement pattern as depicted in Fig. 8.

The active tooth profile can now be pictured as a straight line (on the x coordinate). At each coordinate point it is now possible to evaluate how much energy is released during the meshing cycle based on the data obtained from the contact analysis. Considering that the generated heat losses are split between the contacting bodies we can define a line-distributed

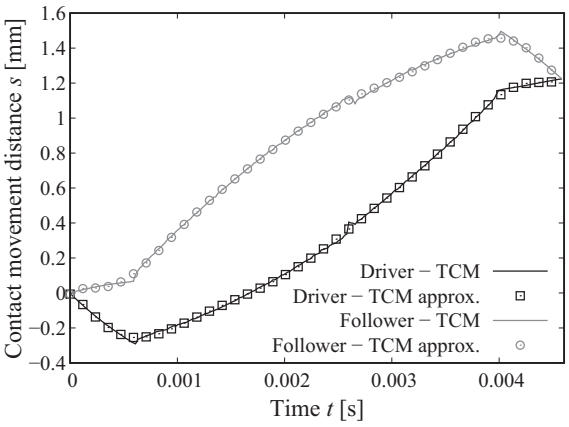

Fig. 8. Evaluated total contact movement path along active tooth flank.

energy function (in J/m), e.g., for the driver gear, as

$$W'_{\mathrm{n},1}(x) = \mu b \int_0^{t_\mathrm{u}} \psi_\mathrm{n}(x) \cdot \underbrace{\{H[x - c_{x1}(t)] - H[x - c_{x2}(t)]\} \cdot p_\mathrm{m}(t) \cdot v_\mathrm{s}(t)}_{f_{\mathrm{n},1}(x,t)} \mathrm{d}t, \tag{12}$$

where c_{x1} and c_{x2} denote the lower and upper boundary locations of the current contact interface. The partitioning $\psi_\mathrm{n}(x)$ can, in this case, be considered as being time independent. The function domain is bounded by $-l/2 \leq x \leq l/2$, where l is the length of the active flank profile. The integral can be rewritten in a reduced manner for both gears as

$$\begin{aligned} W'_{\mathrm{n},1}(x) &= \mu b \int_0^{t_\mathrm{u}} \psi_\mathrm{n}(x) \cdot f_{\mathrm{n},1}(x,t)\mathrm{d}t \\ W'_{\mathrm{n},2}(x) &= \mu b \int_0^{t_\mathrm{u}} [1 - \psi_\mathrm{n}(x)] \cdot f_{\mathrm{n},2}(x,t)\mathrm{d}t \end{aligned} \tag{13}$$

Using these two functions we can construct the heat-flux functions for the subsequent nominal temperature analysis by distributing the energy function across the running cycle time as

$$q_{\mathrm{n},1}(x) = \frac{W'_{\mathrm{n},1}(x)}{b \cdot t_\mathrm{d}} \quad \text{and} \quad q_{\mathrm{n},2}(x) = \frac{W'_{\mathrm{n},2}(x)}{b \cdot t_\mathrm{d}}. \tag{14}$$

The partitioning-coefficient function $\psi_\mathrm{n}(x)$ can be calculated in a similar manner as described in the previous section, the difference being that now the heat losses are distributed across the entire active flank profile and the interface can be considered as static. By temporarily neglecting the partitioning functions in Eqs. (13) and (14), it is possible to directly evaluate the $q_{\mathrm{n},1}(x)$ and $q_{\mathrm{n},2}(x)$ functions. Using these two functions, the nominal temperature rise after an arbitrary amount of time can be evaluated, if all the heat losses are absorbed by one body as

$$\Delta T_\mathrm{n}(x,t) = \frac{1}{2\pi k} \int_0^t \int_{-l/2}^{l/2} \underbrace{\frac{\bar{q}_\mathrm{n}(x')}{t - t'} \exp\left[\frac{(x - x')^2}{4\alpha(t - t')}\right]}_{f_\mathrm{n}} \mathrm{d}x'\mathrm{d}t', \tag{15}$$

where $\bar{q}_\mathrm{n}(x) = [q_{\mathrm{n},1}(x) + q_{\mathrm{n},2}(x)]/2$ is the mean heat-flux function. By partitioning the mean heat-flux function we now obtain

$$\begin{aligned} \Delta T_{\mathrm{n},1}(x,t) &= A_1 \int_0^t \int_{-l/2}^{l/2} \psi_\mathrm{n}(x) f_{\mathrm{n},1}\mathrm{d}x'\mathrm{d}t', \\ \Delta T_{\mathrm{n},2}(x,t) &= A_2 \int_0^t \int_{-l/2}^{l/2} [1 - \psi_\mathrm{n}(x)] f_{\mathrm{n},1}\mathrm{d}x'\mathrm{d}t'. \end{aligned} \tag{16}$$

The partitioning function can then be evaluated using the Gauss quadrature integral solution and constructing a system of equations similar to the one used for the flash-temperature evaluation in Eqs. (8) and (9). After extensive testing we can conclude, however, that both partitioning-coefficient functions $\psi_\mathrm{f}(t)$ and $\psi_\mathrm{n}(x)$ are (if we exclude slight numerical fluctuations) time- and space-independent and can hence be taken as scalar values. The average values of $\bar{\psi}_\mathrm{f}$ and $\bar{\psi}_\mathrm{n}$ also return completely comparable values, so it was concluded that no noticeable error occurs if we apply $\bar{\psi}_\mathrm{f}$ to the functions in Eqs. (13) and (14), which can be used for the nominal temperature analysis described as follows. The evaluated functions for both bodies in contact are presented in Fig. 9.

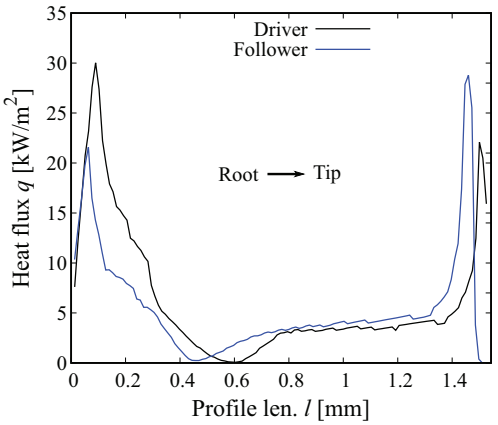

Fig. 9. Heat-flux functions used for the nominal temperature analysis.

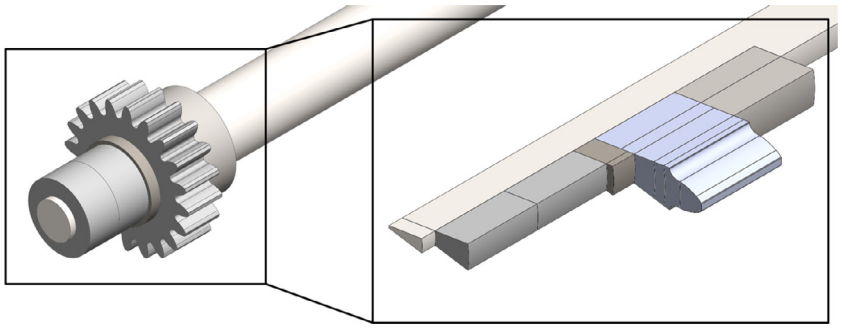

Fig. 10. Reduced CAD geometry considering the cyclic periodicity of the system, used for the nominal temperature analysis.

A minor contributor to the overall temperature rise during gear meshing is the structural heat losses due to the rolling friction. These hysteresis losses are, as noted by Greenwood et al. [32], predominantly located in a sub-surface region, below the contact. They are a consequence of the specific stress state taking place below the contact and are present for rolling and sliding contacts alike. Wannop et al. [33] present a model (based on a description in [32]) for the evaluation of these heat losses during cylinder rolling across a compressible elastic material (Poisson's ratio below $\nu = 0.5$). As the contact body passes across the deformable surface a complex stress state emerges, which can, in a 2D case, be described by a combination of three components: the shear stress $\tau_s = \tau_{xy}$, a secondary shear component $\sigma_s = 0.5 \cdot (\sigma_y - \sigma_x)$ at 45^o from τ_s and the hydrostatic component σ'. Based on the length of the stress path

$$L_\sigma = \int_{-\infty}^{+\infty} \left[\left(\frac{\partial \sigma_s}{\partial x} \right)^2 + \left(\frac{\partial \tau_s}{\partial x} \right)^2 + (1 - 2\nu) \left(\frac{\partial \sigma'}{\partial x} \right)^2 \right] \mathrm{d}x \tag{17}$$

The overall heat-energy loss can be evaluated for $\nu = 0.35$ as

$$W_r = \frac{\beta l b}{8G} \int_0^\infty L_\sigma^2 \ \mathrm{d}y = 0.67 \cdot \beta \frac{F_n c l}{R_c}. \tag{18}$$

Based on [33] the loss factor value $\beta = 0.04$ was considered. The model in our case only serves as an approximate estimate of the hysteresis losses, for which we simplify its implementation by using average values of the parameters in Eq. (18) and by applying the losses directly on the contact surfaces of each gear as a heat flux (energy distributed across the active tooth flank). This was considered acceptable as the resulting values showed that the hysteresis losses represent only 0.5% of the losses due to sliding friction and, hence, make only a minor contribution to the overall temperature rise.

FEM analysis numerical model

Given that the gear geometry and the geometry of the related component in the system, as well as effects like convection, play a major role in the nominal temperature rise, it is most reasonable to perform the temperature evaluation using a FEM. Based on the geometry of the experimental testing rig, presented in the following section in Fig. 12, a CAD analysis model can be constructed, as shown in Fig. 10. In this case the cyclic symmetry of the gear can be exploited to reduce the model to a $1/z$ section. In order to achieve a consistent continuity of the temperature gradient it is very important to impose a cyclic-periodicity condition. The analysis is performed separately for each of the two gears.

Table 5
Parameters of the FE mesh used for the nominal temperature analysis.

Property/Parameter	Value/Tipe
Structural FE [27]	SOLID90
Contact FE [28]	CONTA170/TARGE174
FE size	0.35 mm–0.1 mm
Approximation order	Quadratic
Elem. quality (min./max./mean) [29]	0.15/0.999/0.95
Jacobian ratio (min./max./mean.)	1.0/21.9/1.23

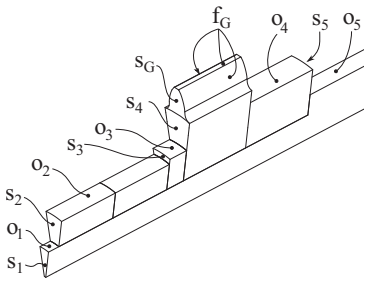

Fig. 11. Division of the outer surfaces exposed to convective effects into characteristic groups.

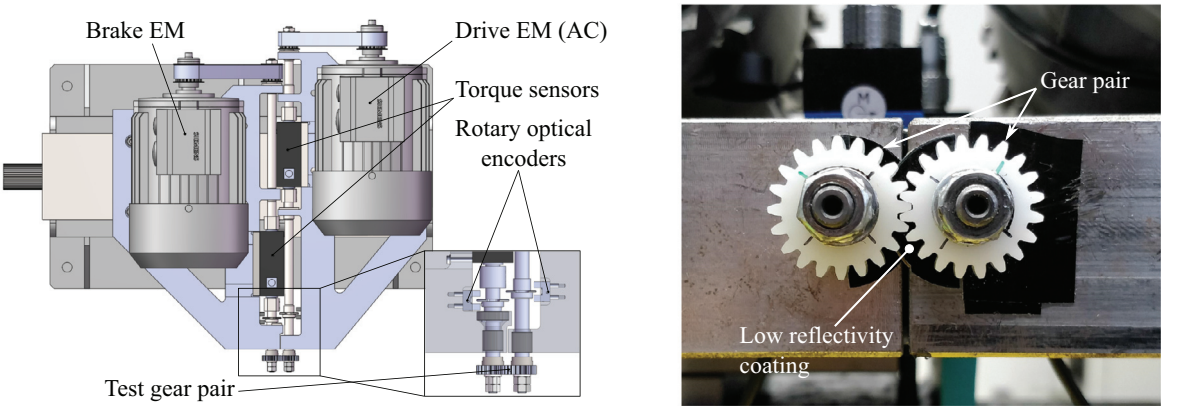

(a) gear testing rig (CAD model) **(b)** Gear pair setup (IR camera perspective)

Fig. 12. Presentation of the testing rig used for temperature measurements.

The thermal load for each gear is applied to the active tooth flank as a time-independent heat-flux function presented in Fig. 9. The main characteristics of the FE mesh based on the presented CAD model are shown in Table 5.

Heat-dissipation mechanisms

The dissipation of the generated heat losses occurs mainly via two processes, i.e., the structural heat conduction and convection. The convective heat dissipation is described in the constitutional heat equation defining the thermal problem using a convective heat-transfer coefficient h that is dependent on the thermal and kinematic properties of the surrounding fluid, i.e., the air. The coefficient can be modeled in two ways, i.e., by using suitable analytical models or by simulating the heat-dissipation process using, e.g., a fluid structure interaction (FSI) type analysis. Given that we want to obtain an as efficient and straightforward model as possible, it is better to use the analytical approach. The first step is to divide the outer surfaces into characteristic groups with similar geometric properties as presented in Fig. 11.

The models used for the evaluation of the heat-transfer coefficient on the cylindrical (o) and side (s) surface types are presented in Table 6. The average Reynolds number is evaluated as $\mathrm{Re}_{\omega,o} = \omega \cdot d^2/(2 \cdot \lambda_{\mathrm{air}})$ for the cylindrical surfaces (o_i), as $\mathrm{Re}_{\omega,s} = \omega \cdot r^2/\lambda_{\mathrm{air}}$ for the side surfaces (s_i) and as $\mathrm{Re}_{v,d} = v_0 \cdot L/\lambda_{\mathrm{air}}$ for the tooth side (s_G). For the latter, v_0 is the pitch circle velocity and L is the mean tooth thickness. It should be stressed that it is important to model the tooth's side surface separately from the surfaces of the lower gear body (as opposed to the models considered in [12] and [11]) as this leads to a much more accurate representation of the tooth's temperature gradient. The cylindrical surface o_2 actually represents a hexagonal nut, for which we can expect a somewhat increased convection effect. The Nusselt number for this surface type and for $\mathrm{Re}_{\omega,o} < 1000$ can be approximately modeled as $0.49 \cdot \mathrm{Re}_{\omega,o}^{1/2}$.

Table 6
Evaluation of the convective heat-transfer coefficient for different surface types at different Reynolds numbers.

Par.	Cylindrical surfaces (o_i)		Side surface (s_i)	Tooth side (s_G)
Re	$\mathrm{Re}_{\omega,o}<1000$	$\mathrm{Re}_{\omega,o} \geq 1000$	$4 \leq \mathrm{Re}_{\omega,s} \leq 2 \cdot 10^6$	$< 5 \cdot 10^5$
Nu	Free convection	$0.533 \cdot \mathrm{Re}_{\omega,o}^{1/2}$ [34]	$0.326 \cdot \mathrm{Re}_{\omega,s}^{1/2}$ [35,36]	$0.664 \cdot \mathrm{Re}_{v,d}^{1/2} \cdot \mathrm{Pr}^{1/3}$ [37]
h	≈ 10 W/(m^{2}K)	$\frac{\mathrm{Nu} \cdot k_{\mathrm{air}}}{d}$	$\frac{\mathrm{Nu} \cdot k_{\mathrm{air}}}{r}$	$\frac{\mathrm{Nu} \cdot k_{\mathrm{air}}}{L}$

The convection through the gear-flank surfaces (f) can be analytically described using the equation

$$\mathrm{Nu} = \frac{2h_{\mathrm{c,f}} \cdot r_{\mathrm{k}}}{k_{\mathrm{air}}} = C_{\mathrm{h}} \left(\frac{2\nu_0 r_{\mathrm{k}}}{\lambda_{\mathrm{air}}} \right)^{n_{\mathrm{h}}} \mathrm{Pr}^{1/3}, \tag{19}$$

as defined in [38]. Here, r_{k} is taken as the tooth height (i.e., $r_{\mathrm{k}} = (d_{\mathrm{a}} - d_{\mathrm{b}})/2.0 = 1.56$ mm). In [37] the authors gather the values for the coefficients C_{h} and n_{h} for different profile geometries. The convective coefficient for the gear-tooth geometry was found to be suitably approximated by applying the coefficients $C_{\mathrm{h}} = 3.8$ and $n_{\mathrm{h}} = 0.2$. It can be presumed that the reduced convection during gear meshing does not influence the overall dissipation process, as the meshing time is very small compared with the entire running cycle.

The structural heat dissipation is dependent on the thermal conductivity of the materials, but also on the thermal contact conductance between the adjoining components. Based on a thorough literature research the conclusion was drawn that the most suitable model to evaluate the contact conductance coefficient was the Mikić model described in [39]. The contact deformation between the asperities of two components can either be predominantly elastic or predominantly plastic. A criterion for the evaluation of the predominant type of contact deformation is put as

$$\chi = \frac{H_{\mathrm{m}}}{E_{\mathrm{c}} \tan(\theta_{\mathrm{c}})}. \tag{20}$$

For $\chi \leq 0.33$ the asperities deform elastically, while for $\chi \geq 3$ the deformations are plastic. Between these values the deformation are elasto-plastic. The contact conductance coefficient for the plastic deformations can be evaluated as

$$h_{\mathrm{s}}^{\mathrm{p}} = 1,13 \frac{k_{\mathrm{c}} \cdot \tan(\theta_{\mathrm{c}})}{\sigma_{\mathrm{c}}} \left(\frac{p_{\mathrm{c}}}{H_{\mathrm{m}}} \right)^{0,94}, \tag{21}$$

where k_{c} is the combined thermal conductivity coefficient $k_{\mathrm{c}} = (2k_1k_2)/(k_1 + k_2)$, while σ_{c} is the combined RMS roughness of the contacting surfaces $\sigma_{\mathrm{c}} = \sqrt{\sigma_{\mathrm{s1}}^2 + \sigma_{\mathrm{s2}}^2}$. For elastic deformations the coefficient becomes

$$h_{\mathrm{s}}^{\mathrm{e}} = 1,55 \frac{k_{\mathrm{c}} \tan(\theta_{\mathrm{c}})}{\sigma_{\mathrm{c}}} \left(\frac{p_{\mathrm{c}}\sqrt{2}}{E_{\mathrm{c}} \tan(\theta_{\mathrm{c}})} \right)^{0,94}. \tag{22}$$

3. Experimental work

The presented analysis procedure needs to be thoroughly validated through suitable experimental tests. As mentioned, the considered gear geometry used for the FEM analyses was taken based on the geometry of the samples used for gear running tests on in-house-developed testing equipment.

The composition of the available testing rig is shown in Fig. 12. The rig enables the set-up and active control of any combination of torque and running speed in the range 0.1–1.7 Nm and 600–2000 min^{-1}. The rig is located in a thermal chamber where the surrounding air temperature can be set between 15 and 30 °C (± 1.5 °C). During the measurements the air temperature and humidity are constantly measured.

The used samples, as defined in Table 2, were machined from extruded rods. The temperature measurements during the tests were performed using a Thermosensorik CMT 384SM high-speed IR camera. In the used set-up, the camera has an ≈ 1912 fps frame rate, with an integration time of 0.1 ms, in a 64 × 64 px window, enough to clearly capture each separate tooth in a static frame during running. The gear-rotation speeds defined in Table 3 were chosen relative to the camera's frame rate, so that a given frame capture set can be presented as a static picture, where each subsequent frame depicts the next gear tooth at the same position as the previous one. The thermal calibration of the camera was made using a high-precision calibration plate, onto which a thin plate of each of the used polymer materials was heated to a specific temperature and used as a reference for the calibration. In order to reduce the infrared (IR) reflection from the background surfaces that could produce unrealistic results during the gear temperature measurements, a pair of Acktar Metal Velvet™ low-reflectivity coating stickers was applied to the surfaces behind the gears (Fig. 12b).

Using the described testing equipment, detailed temperature measurements of the gear teeth during running can be obtained. As shown in Fig. 13, it is possible to observe the evolution of the temperature field from two perspectives. One is the time-dependent nominal temperature rise at a chosen reference point (Fig. 13a). For this, a very small square portion on the side surface at a reference radius r_{r}, about 0.25 mm below the tooth root radius was chosen. The second measurement method is the frame-capture method where the entire temperature gradient present on the gear's side surface can be

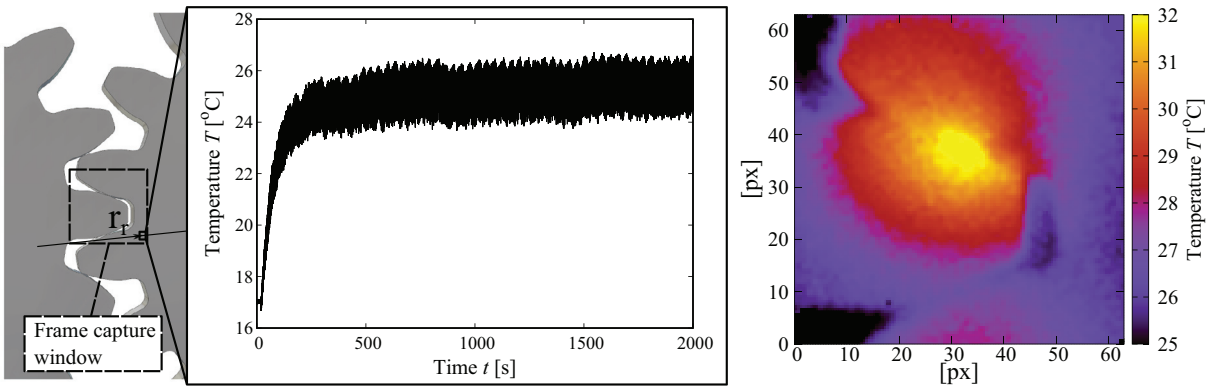

(a) Time-dependent temperature measurements (b) Frame-capture measurements

Fig. 13. Experimental temperature measurements during gear running. Measurements taken at a running torque $M \approx 0.6$ Nm and a running speed $n = 1147$ min^{-1}.

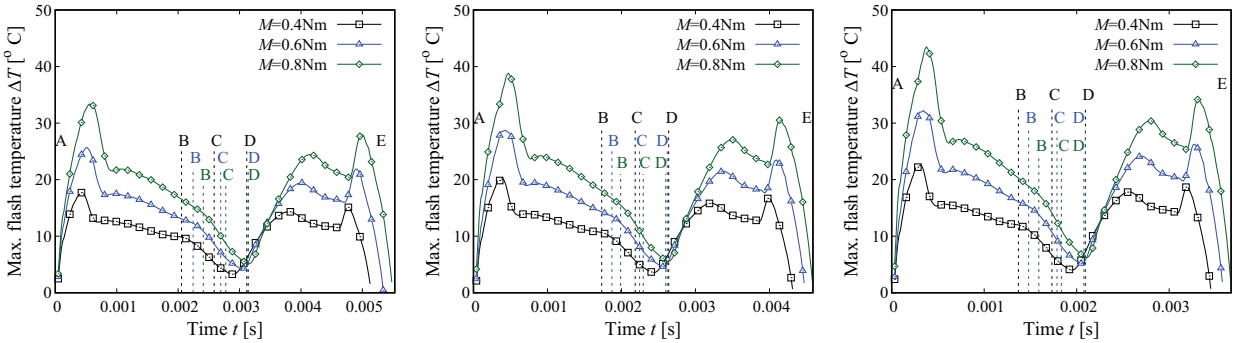

(a) $n = 956\text{min}^{-1}$ (b) $n = 1147\text{min}^{-1}$ (c) $n = 1434\text{min}^{-1}$

Fig. 14. Flash-temperature results for the considered load cases.

measured, as presented in Fig. 13b. The capture sequence is carried out in such a way that each consecutive snap is taken right after a $\delta = 360^o/z$ rotation of the gears. In the figure we used a linear interpolation between measurement points (2 intermediate points used) in order to increase the visual resolution of the picture.

The validation of the model presented in the previous sections will be carried out based on the two just-described measurement methods.

4. Results and discussion

4.1. Flash temperature using the semi-analytical model

Using the presented flash-temperature model for the profile geometry presented in Fig. 2b and the considered load configurations (Table 3) we can calculate the peak local time-dependent temperature rise patterns during a meshing cycle at the contact interface, as depicted in Fig. 14. These results should be taken as the temperature rise above the nominal temperature component (which can be viewed as the root temperature). As expected, a clear dependence on the running speed and applied torque is exhibited. Also evident is the fact that the local temperature due to frictional losses rises very quickly to a relatively substantial magnitude at the points of increased contact pressure and sliding speed. The resulting temperature peaks, however, also dissipate rather quickly, leaving a substantially diminished temperature gradient behind the contact interface. It should be noted, however, that it is most likely that the peak temperatures at the beginning and end of the meshing would be lower than those predicted by the model due to the accumulated strain and retardation effects present in the polymers, which would lead to slightly lower contact pressures. Additional remarks regarding the presented results are noted in Section 4.3.

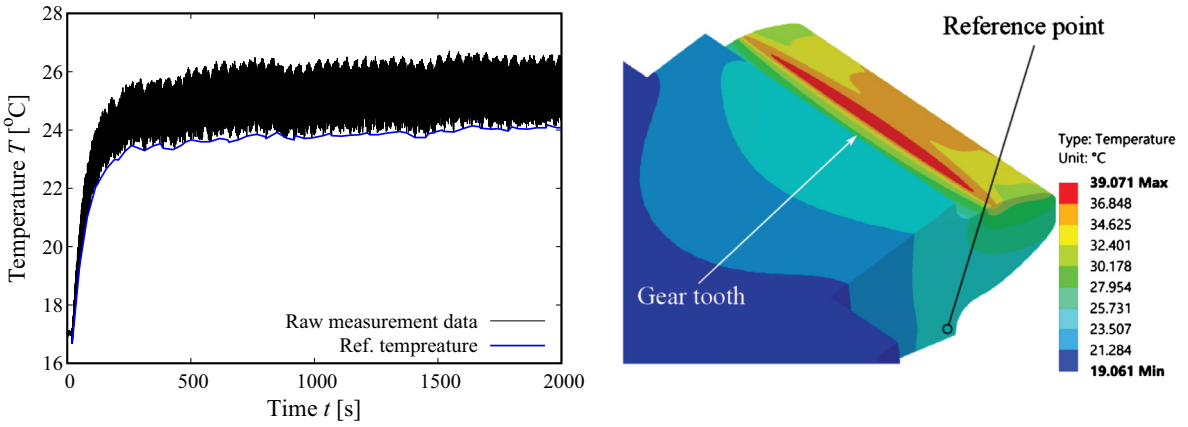

(a) Experimental reference **(b)** Model reference point

Fig. 15. Selected experimental and model reference points for the nominal temperature comparison between the measured and evaluated results (nominal load: $M = 0.6$ Nm, $n = 1147$ min^{-1}).

4.2. FEM Thermal analysis results

As defined in Table 3, three different running speeds and torques were considered in our tests and analyses, together forming nine different load combinations. The time-dependent nominal temperature measurements typically show a considerable degree of scatter, as evident in Fig. 15a. This happens for two reasons. First, the camera frame rate could not be set precisely to one value, hence, a slight degree of angular shift is present during the measurements. Second, as will be presented in the following section, geometric deviations can have a significant influence on the temperature field for different tooth pairs. In order to have a suitable reference point for a comparison with model computations, we will observe the bottom measurement points occurring during separate fluctuation periods (blue line in Fig. 15a), which should coincide with the tooth pair closest to a theoretical gear geometry (exhibiting the optimum meshing kinematics) and the point on the measurement radius r_r furthest away from the meshing flanks (see Fig. 15b).

By considering this comparison approach the experimental and model results can be plotted separately for each of the three considered running speeds, as presented in Fig. 16.

The experimental results are plotted using error bars that represent the deviations between the temperature measurement repetitions at the same running loads (3 repetitions performed for each load configuration). In general, the model results show good agreement with the experiment in the considered testing times. However, several characteristic aspects and discrepancies between the model and the real-life behavior of the gear pair were noticed that need to be addressed at this point. First of all, a scatter in the measured temperatures was observed if longer testing times are applied, independent of the considered loading conditions. While some test samples achieved a plateau-like steady state in the observed time window, others showed a constant temperature increase that lasted for several hours before a quasi-steady state was reached (e.g., the $M = 0.8$ Nm test in Fig. 16f). For higher loads (above 1 Nm) this continuous rise can even persist till the failure of one of the samples. This type of behavior points to intrinsic non-linearities in the system, where the temperature-dependent thermo-mechanical properties of the material and the nonlinear contact properties of the material pair can play an important role in the system's response. Furthermore, it is very likely that the geometric tolerance deviations vary from sample to sample, which in the case of a tooth pair with unfavorable tolerance deviations in the meshing can result in higher contact pressures, sliding speeds and resulting heat losses. Also, high structural stresses can result in non-elastic strain accumulation that would also result in alterations to the gear kinematics and possibly in even greater thermal losses. This can, consequently, meaningfully drive up the temperature field of the entire gear pair. The described effects can to a certain degree be considered also in a thermo-mechanical model; however, it is extremely difficult to simultaneously account for all of these effects in one model. Some additional remarks on this point are included in the following pages. We can also see that the model shows faster heating than the measurements. This can, in small part, be due to the initial ramp increase of the running torque after the test start. It was also hypothesized that this could be a consequence of an inconstant COF, that could vary with increasing temperature (as well as with the contact pressure and sliding speed).

We can now examine in more detail the thermal behavior of individual tooth pairs by analyzing the data obtained from the frame-capture measurements, as described in the previous section (see Fig. 13b). A comparison of the measured and computed temperature gradient at the gear's side surface is presented in Fig. 17a and b, respectively. In both cases a noticeable temperature gradient is present around the active tooth flank. It can be seen, however, that the numerical results overestimate the temperature, as compared to the measurements (at the current point of contact the measurements show an about 25% lower temperature rise than the model). This is probably due to the fact that around the flank edge the convection effect is increased as compared to the rest of the tooth side surface. It is also possible that the local peaks are not

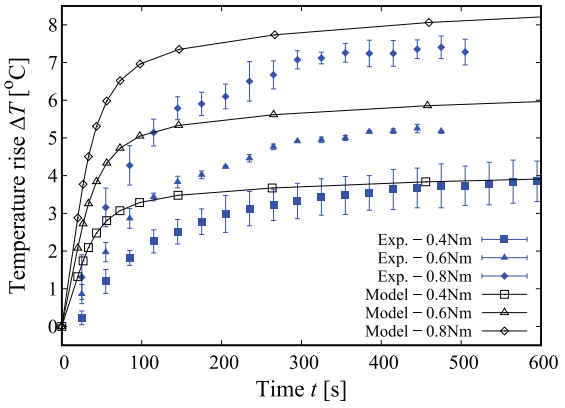

(a) Running speed $n = 956\text{min}^{-1}$ and variable torques

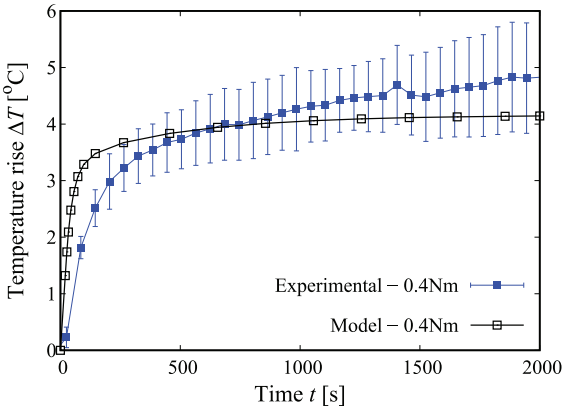

(b) Prolonged testing time ($t = 2000$s) - Running speed $n = 956\text{min}^{-1}$ and torque $M = 0.4$Nm

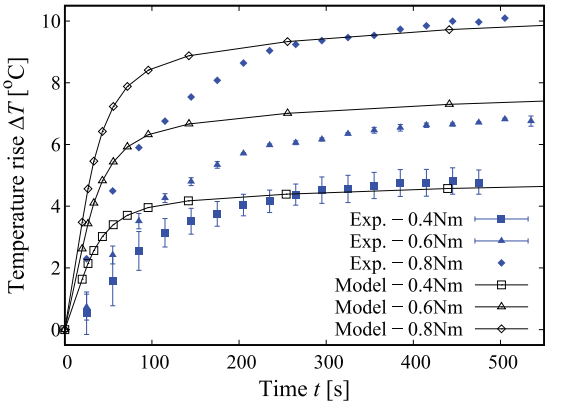

(c) Running speed $n = 1147\text{min}^{-1}$ and variable torques

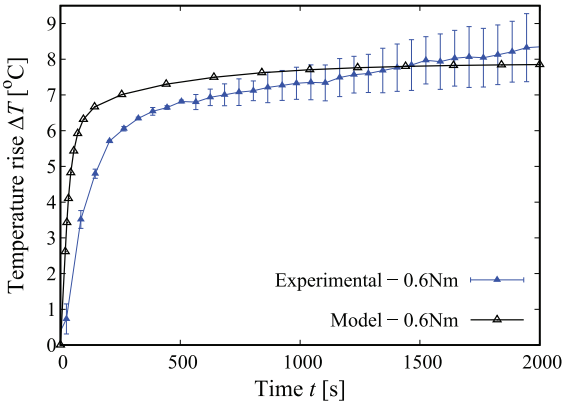

(d) Prolonged testing time ($t = 2000$s) - Running speed $n = 1147\text{min}^{-1}$ and torque $M = 0.6$Nm

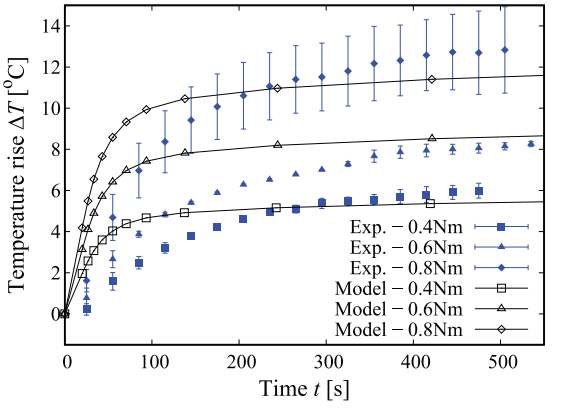

(e) Running speed $n = 1434\text{min}^{-1}$ and variable torques

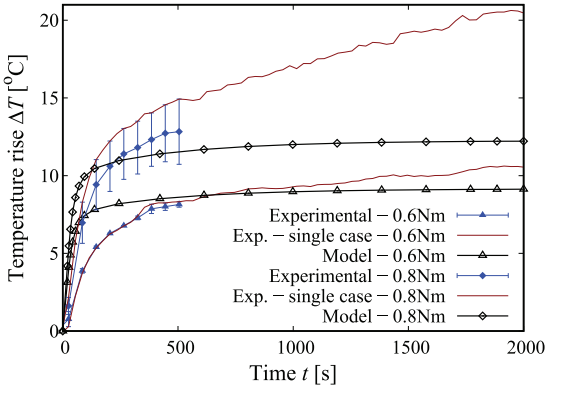

(f) Prolonged testing time ($t = 2000$s) - Running speed $n = 1434\text{min}^{-1}$ and torques $M = 0.6$Nm and $M = 0.8$Nm

Fig. 16. Comparison between the experimental and model results evaluated for the defined reference points for variable combinations of running speeds and torques.

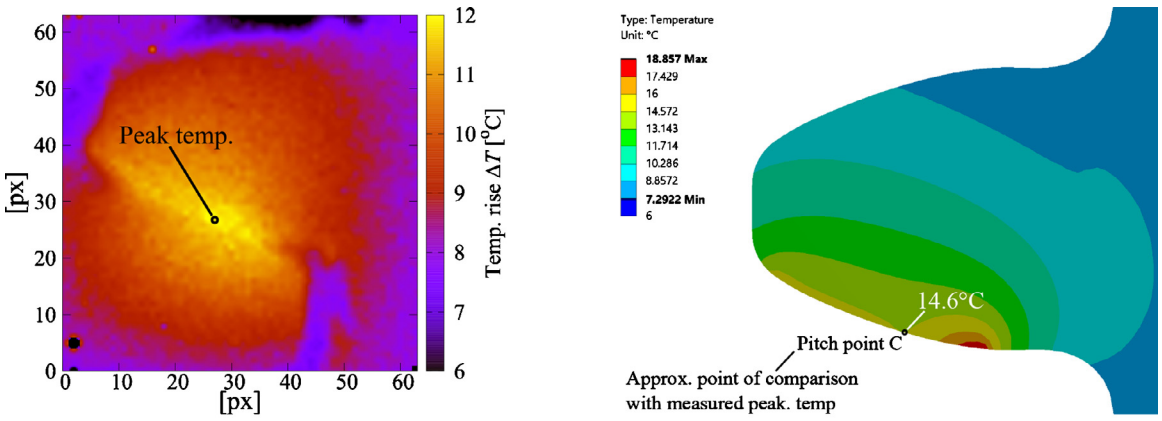

Fig. 17. Comparison between frame-capture temperature measurements using the high-speed thermal imaging camera and numerical analysis results at the gear's side surface ($M = 0.6$ Nm; $n = 1147\,\mathrm{min}^{-1}$).

fully captured due to the relatively low camera resolution. Additionally, it is presumed that due to the temperature rise the materials lose their stiffness to a certain degree, distributing the contact load over a larger contact area and decreasing the local peak temperature. The overall peak temperature is anyhow located at the middle tooth thickness, near the base circle diameter and is noticeably higher than the temperature at the side surface. A third observation drawn from the measurements is that a continuous temperature gradient is present at the contact throughout both teeth, which confirms the assumption of an equal contact temperature used for the evaluation of the heat partitioning coefficient (Černe et al. [17]). Based on our findings, it can be concluded that the FEM does not only provide information regarding the nominal temperature (i.e., at the tooth root) but also represents rather faithfully the instantaneous flash-temperature rise, even though in the model a steady time-independent heat flux is prescribed.

Thermal measurements for the root-temperature validation were mostly performed in the phase just after meshing completion, so as to exclude any unwanted influences from the local temperature rise. Here, the temperature gradient phases out almost entirely, with temperatures remaining only slightly above the values measured at the root. One occurrence that was also observed in virtually all the tests was the noticeable deviation in the temperature rises between separate tooth pairs. In Fig. 18 a comparison between the highest and lowest measured tooth-temperature fields during a single running cycle after approximately $t = 600$ s running time in three different load configurations is presented. As visible, in all three measurements a marked discrepancy is recorded between the minimum and maximum tooth-pair temperature fields. This variation can, based on preliminary analyses, be attributed to different geometric-tolerance deviations present for the individual tooth pairs. The effects of geometric deviations on the tooth profile should be studied more thoroughly in future work, in order to provide more definitive conclusions on this topic. In our thermo-mechanical model they can most simply be accounted for by applying a suitable scaling factor to the evaluated temperature results. Based on the so-far conducted measurements an upscaling factor of between 1.25 and 1.3 should be applied.

The final structure of the developed model can be presented in a schematic way, as shown in Fig. 19. As already pointed out the FEM thermal analysis used for nominal temperature evaluation also provides consistent flash-temperature results (based on experimental observations). The implementation of the semi-analytical flash-temperature model is, however, still necessary as it enables the evaluation of the heat-partitioning coefficient ψ_f.

4.3. Limitations of the considered presumptions and methodology

In our analysis an array of presumptions was considered that enabled us to construct a fairly physically consistent, but still relatively efficient, model. Based on our analysis of the structural deformation losses we could confirm that the main driver of the temperature rise is the sliding friction losses. An additional analysis of the structural losses present throughout the tooth (i.e., considering fatigue losses at the root) should still be carried out, but they are not expected to alter the results in any significant way.

Most existing polymer gear temperature models presume a constant COF (see e.g. Mao [8], Blok [7], Casanova et al. [18] or Fernandes et al. [12] - dry running case). In the research by Doll [14] the influence of sliding speed, pressure and temperature on the COF of PEEK-PEEK and Steel-PEEK material pairs was studied. Even though the author does acknowledge the influence of these parameters on the COF, a constant COF value (taken as an average of the measured values) was still considered in the described numerical analysis. The sliding frictional losses should in any case be studied more thoroughly to assess whether the presumption of a constant COF is realistic or not. As was seen in the nominal temperature results in Fig. 16, the model predicts a noticeably faster temperature rise than was observed in the measurements. It is presumed that

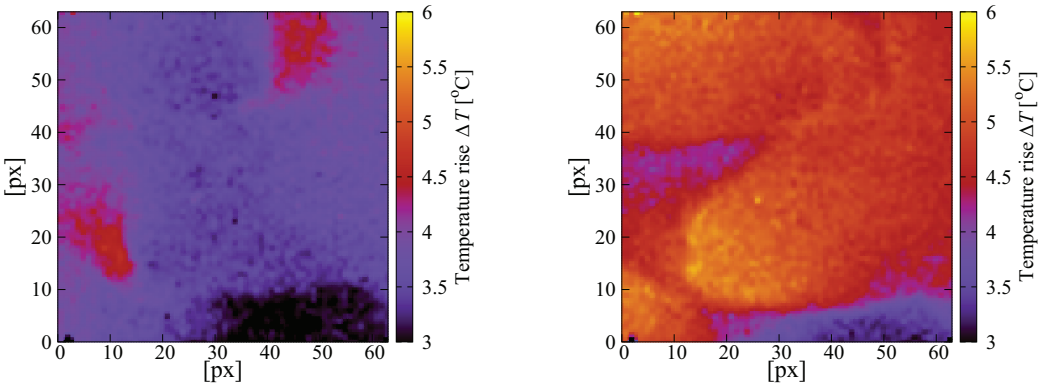

(a) Load cond.: $n = 956\text{min}^{-1}$, $M = 0.4\text{Nm}$ - lowest tooth temperature

(b) Load cond.: $n = 956\text{min}^{-1}$, $M = 0.4\text{Nm}$ - highest tooth temperature

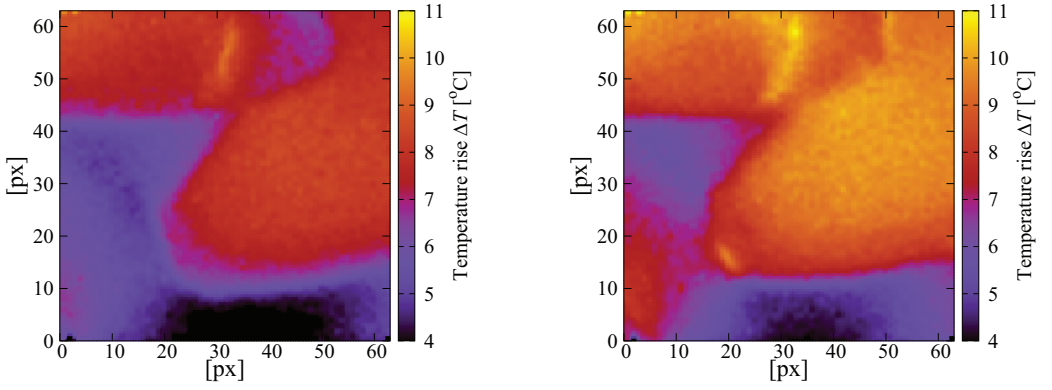

(c) Load cond.: $n = 1147\text{min}^{-1}$, $M = 0.6\text{Nm}$ - lowest tooth temperature

(d) Load cond.: $n = 1147\text{min}^{-1}$, $M = 0.6\text{Nm}$ - highest tooth temperature

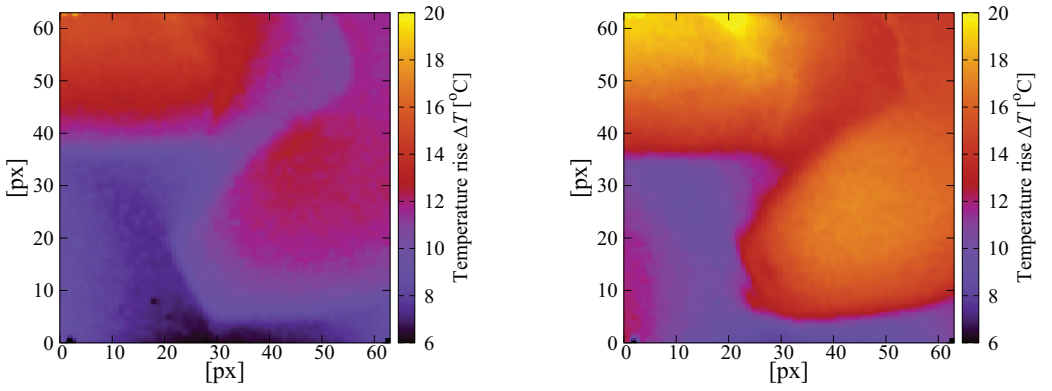

(e) Load cond.: $n = 1434\text{min}^{-1}$, $M = 0.8\text{Nm}$ - lowest tooth temperature

(f) Load cond.: $n = 1434\text{min}^{-1}$, $M = 0.8\text{Nm}$ - highest tooth temperature

Fig. 18. Examination of the temperature gradient on the gear teeth during running. Lowest and highest recorded temperature fields at the tooth side surfaces during a single gear running cycle taken after approximately $t = 600$ s running period.

the frictional losses begin to increase with time due to a change in the COF with time (as was noted by Pogačnik et al. in [40] and [41]).

It would, as a result, be advisable to assess the time- and temperature-dependent behavior of the COF for the considered material pair. While an implementation of a temperature/pressure/sliding velocity dependent COF inside our model is possible (and also planned as part of future research), a suitable COF characterization needs to be carried out. Our current findings also point to the fact that common tribological testing methods like pin-on-disk do not represent faithfully enough the tribological nature of (polymer) gears. In a pin-on-disk (or block-on-ring) test, for example, the contact surface of the

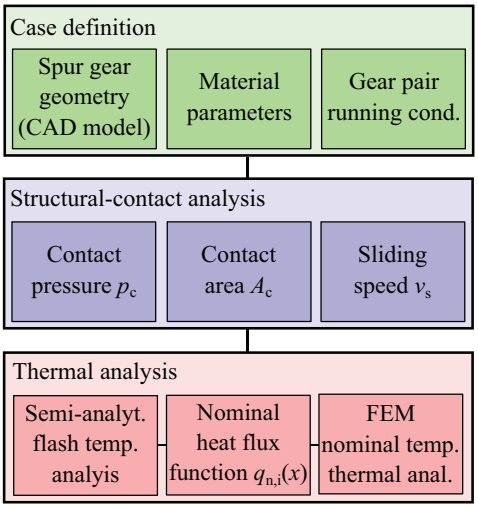

Fig. 19. Schematic representation of the developed model's structure.

pin is in constant sliding contact and is, hence, constantly exposed to frictional load with corresponding thermal losses. On the other hand, during gear meshing the contact position is constantly changing on both bodies and a combination of sliding and/rolling is present throughout the cycle. A test procedure with more similar sliding/rolling conditions to the ones present during gear meshing should therefore be applied, in order to properly characterize the COF, in accordance with the contact conditions present during gear meshing. We assume that an approach similar to the one taken by Hoskins et al. [42] would yield much more realistic results.

Perhaps the most important and problematic assumption in our model is the thermo-mechanical temperature independence of the model. This enabled us to keep at least the material linearity of the model, and perform the evaluation in an efficient sequential manner, as compared to a coupled thermo-mechanical analysis that would be extremely computationally expensive (not even possible without an HPC cluster). It does not, however, take away from the fact that the behavior of thermoplastics is, in most cases, markedly temperature dependent, especially in terms of mechanical behavior. An analysis of the influence of temperature on the mechanical strength of the material and the consequent influence on the heat losses is still due at this point, but it will be carried out shortly. It can, however, be concluded, based on the presented results, that the presumption still allows us to obtain reasonably accurate results in the considered running time frame.

Along with the just-mentioned presumption, we also considered the polymers as being linearly elastic. It is known that the thermoplastic behavior is in most cases constitutionally viscoelastic, i.e., time/rate dependent, and that the viscous component of the material can meaningfully influence the material's response. So far the Generalized Maxwell and Generalized Voigt models were considered in our mechanical analyses but, for a single meshing cycle, the difference, as compared to the elastic model, was minimal. A more long-term analysis, with a larger number of load cycles, would presumably show a much more meaningful influence of the viscoelastic part, but such analyses can prove to be difficult to validate, with the materials requiring a specific type of characterization, as well as being computationally demanding. In such analyses the temperature influence would also need to be taken into account, which again complicates the procedure substantially. It is, however, very likely that the non-elastic properties of the material contribute to the fact that the gear temperature does not quite reach a completely steady state in the expected time frame (even when applying low load levels). For this reason the applicability of the model is limited to shorter running times, i.e. in the studied case, below $t = 2 \cdot 10^3$ s. Given that most existing polymer gear applications do not, on average, run even nearly that long this can be considered an acceptable limitation.

While in our FEM thermal analysis the effect of convective heat dissipation was considered, this effect is not included in the semi-analytical flash-temperature model. As is evident from the measurements, convection does seem to hold an important role in driving down the temperature rise, even though the meshing time is rather small compared to the overall running cycle. The results based on the semi-analytical model hence turn out to be somewhat conservative.

The considered gear case with $i = 1$ ensures that the same tooth pairs are always meshing. While this type of gearing is not typical in real-life applications, it enables us to observe how geometric deviations might influence the heat losses. A consequence of this choice is, however, also greater instability of the system. If an unfavorable tooth pair with higher deviations comes into a constant mesh it will drive the temperature of the whole gear up and presumably also prevent the system from reaching a steady temperature state, or delay it by an amount of time (see, e.g., results for $M = 0.8$ Nm in Fig. 16f). It is very likely that if higher transmission ratios are used, with uneven numbers of teeth on the gears, greater stability of the system would be attained.

5. Conclusion

To sum up, the key conclusions that can be drawn from the presented research are:

- The overall temperature rise during gear running is predominantly due to the sliding frictional heat losses (for the considered case rolling friction accounts for approximately only 0.5% of the losses).
- The temperature rise is suitably described by splitting it into the nominal temperature and flash-temperature components.
- The nominal temperature can be equated to the tooth-root temperature. Outside the meshing cycle the temperature is, at least for the running times considered here, fairly homogeneous throughout the tooth structure.
- The presented numerical analysis approach offers a reliable method for the evaluation of the temperature rise during gear running and also provides an efficient tool for the optimization of a gear pair from a thermal standpoint.
- A noticeable temperature gradient is present around the active tooth flanks during gear meshing, which is regarded here as the flash-temperature rise. The presented semi-analytical flash-temperature model provides a somewhat conservative estimation of the flash temperature, as it does not consider the local convective heat dissipation. A more consistent representation is given by the thermal FEM using a set of steady boundary conditions and loads.
- Tolerance deviations from the ideal tooth-profile geometry can lead to higher heat losses and a higher temperature rise than predicted.
- High speed thermography proved to be an essential tool in our thermal analysis and model validation as it provides the chance to study in detail the thermal response of the gear pair during running.

The presented model equips us with an efficient tool for the thermal analysis of polymer gears and offers the chance to study the influence of the considered gears' material behavior and (macro as well as micro) geometry, along with the influence of any adjacent components. In the current form it serves as a backbone for further analyses and upgrades, where especially the effects of temperature, sliding speed and other parameters on the COF should be studied more thoroughly. An additional goal is to obtain a better insight into the long-term influence of the non-elastic properties of the considered polymers on the gearing kinematics, the contact behavior and, consequently, the time-dependent thermal losses. Furthermore, a detailed experimental and analytical study of the influence of geometric deviations (profile modifications and tolerance deviations) will be carried out as part of our future research.

Declaration of Competing Interest

The authors declare that they do not have any financial or nonfinancial conflict of interests.

Acknowledgments

This work was partly financed by the Slovenian Research Agency (ARRS; evidence no. 37664, program code P2-0256 and contract no. 630-33/2019-1) and funded in part by the MAPgears project (co-financed by the Republic of Slovenia and the European Union under the European Regional Development Fund, contract no. C3330-18-952014). We would also like to thank Prof. PhD. M. Dular from the Laboratory for Hydraulic Machines, Faculty of Mechanical Engineering, Ljubljana, for providing crucial experimental equipment for the presented experimental part of the research.

References

[1] VDI 2736-Part 1:2016-07, Thermoplastic Gear Wheels - Materials, Material Selection, Production Methods, Production Tolerances, form Design, Standard,
[2] VDI 2736-Part 2:2014-06, Thermoplastic Gear Wheels - Cylindrical Gears - Calculation of the Load-Carrying Capacity, Standard.
[3] H. Hachmann, E. Strickle, Polyamide als zahnradwerkstoffe, Konstruktion 18 (1966) 81–94.
[4] S. Beermann, VDI 2736 - new guideline, old challenges, in: International Conference on Gears 2015, VDI-Berichte; 2255, 2015, pp. 1231–1240.
[5] A. Pogačnik, J. Tavčar, An accelerated multilevel test and design procedure for polymer gears, Mater. Des. 65 (2015) 961–973, doi:10.1016/j.matdes.2014.10.016.
[6] F.E. Kennedy, Y. Lu, I. Baker, Contact temperatures and their influence on wear during pin-on-disk tribotesting, Tribol. Int. 82 (2015) 534–542, doi:10.1016/j.triboint.2013.10.022.
[7] H. Blok, The flash temperature concept, Wear 6 (6) (1963) 483–494, doi:10.1016/0043-1648(63)90283-7.
[8] K. Mao, A numerical method for polymer composite gear flash temperature prediction, Wear 262 (11) (2007) 1321–1329, doi:10.1016/j.wear.2007.01.008.
[9] S. Takanashi, A. Shoi, On the temperature risk in the teeth of plastic gears, in: International Power Transmission and Gearing Conference, San Francisco, 1980.
[10] G. Erhard, Designing with plastics, Carl Hanser Verlag, Munich, 2006.
[11] B. Luo, W. Li, Influence factors on bulk temperature field of gear, Proc. Inst. Mech.Eng. Part J J. Eng. Tribol. 231 (8) (2017) 953–964, doi:10.1177/1350650116684275.
[12] C.M.C.G. Fernandes, D.M.P. Rocha, R.C. Martins, L. Magalhães, J.H.O. Seabra, Finite element method model to predict bulk and flash temperatures on polymer gears, Tribol. Int. 120 (2018) 255–268, doi:10.1016/j.triboint.2017.12.027.
[13] P.M. Marques, R.C. Martins, J.H. Seabra, Power loss and load distribution models including frictional effects for spur and helical gears, Mech. Mach. Theory 96 (2016) 1–25, doi:10.1016/j.mechmachtheory.2015.09.005.
[14] N.P. Doll, Modeling Thermomechanical Behavior of Polymer Gears, University of Wisconsin-Madison, 2015, doi:10.13140/RG.2.1.2838.2563.
[15] B. Černe, J. Duhovnik, Semi-analytical method for the prediction of the flank temperatures of polymer gears during running, in: Proceedings of the VDI International Conference on High Performance Plastic Gears, Garching, 2017.

[16] B. Černe, D. Zorko, J. Duhovnik, J. Tavčar, R. Žavbi, Flash temperature analysis method for polymer gears with consideration of deviations in meshing kinematics, in: 2019 International Power Transmission and Gearing Conference, Vol. 10, 2019, doi:10.1115/DETC2019-97824.
[17] B. Černe, J. Duhovnik, J. Tavčar, Semi-analytical flash temperature model for thermoplastic polymer spur gears with consideration of linear thermo-mechanical material characteristics, J. Comput. Des. Eng. (2019), doi:10.1016/j.jcde.2019.03.001. In press.
[18] V. Roda-Casanova, F. Sanchez-Marin, A 2D finite element based approach to predict the temperature field in polymer spur gear transmissions, Mech. Mach. Theory 133 (2019) 195–210, doi:10.1016/j.mechmachtheory.2018.11.019.
[19] K. Mao, W. Li, C. Hooke, D. Walton, Polymer gear surface thermal wear and its performance prediction, Tribol. Int. 43 (1) (2010) 433–439, doi:10.1016/j.triboint.2009.07.006.
[20] D. Zorko, S. Kulovec, J. Tavčar, J. Duhovnik, Different teeth profile shapes of polymer gears and comparison of their performance, J. Adv. Mech. Des. Syst. Manuf. 11 (6) (2017) JAMDSM0083–JAMDSM0083, doi:10.1299/jamdsm.2017jamdsm0083.
[21] D. Zorko, S. Kulovec, J. Duhovnik, J. Tavčar, Durability and design parameters of a steel/peek gear pair, Mech. Mach. Theory 140 (2019) 825–846, doi:10.1016/j.mechmachtheory.2019.07.001.
[22] E. Letzelter, M. Guingand, J.-P. de Vaujany, P. Schlosser, A new experimental approach for measuring thermal behaviour in the case of nylon 6/6 cylindrical gears, Polym. Test. 29 (8) (2010) 1041–1051, doi:10.1016/j.polymertesting.2010.09.002.
[23] ISO 527-2:2012, Plastics – Determination of tensile properties – Part2: Test conditions for moulding and extrusion plastics.
[24] Cylindrical gears for general and heavy engineering – Standard basic rack tooth profile, ISO 53, 1998-08.
[25] System of Gear Fits; Backlash, Tooth Thickness Allowances, Tooth Thickness Tolerances; Principles, DIN 3967, 1978-08.
[26] Cylindrical gears – ISO system of accuracy, ISO1328, 1997.
[27] ANSYS Mechanical APDL 2019 R3, Element reference.
[28] ANSYS Mechanical APDL 2019 R3, Contact Technology Guide.
[29] ANSYS Meshing 19.1, Meshing User's guide.
[30] J.A. Williams, R.S. Dweyer-Joyce, Contact between solid surfaces, in: B. Bhushan (Ed.), Modern Tribology Handbook, Two volume set, CRC Press, Boca Raton, 2000.
[31] W. Li, P. Zhai, J. Tian, B. Luo, Thermal analysis of helical gear transmission system considering machining and installation error, Int. J. Mech. Sci. 149 (2018) 1–17, doi:10.1016/j.ijmecsci.2018.09.036.
[32] J.A. Greenwood, H. Minshall, D. Tabor, Hysteresis losses in rolling and sliding friction, Proc. R. Soc. London A 259 (1299) (1961) 480–507, doi:10.1098/rspa.1961.0004.
[33] G.L. Wannop, J.R. Archard, Elastic hysteresis and a catastrophic wear mechanism for polymers, Proc. Inst. Mech.Eng. 187 (1) (1973) 615–623, doi:10.1243/PIME_PROC_1973_187_147_02.
[34] A.A. Kendoush, An approximate solution of the convective heat transfer from an isothermal rotating cylinder, Int. J. Heat Fluid Flow 17 (4) (1996) 439–441, doi:10.1016/0142-727X(95)00002-8.
[35] K. Millsaps, K. Pohlhausen, Transfer by laminar flow from a rotating plate, J. Aeronaut. Sci. 19 (1952) 120–126, doi:10.2514/8.1955.
[36] G. Cardone, T. Astarita, G.M. Carlomagno, Heat transfer measurements on a rotating disk, Int. J. Rotating Mach. 3 (1) (1997) 1–9, doi:10.1155/S1023621X97000018.
[37] J.P. Holman, Heat Transfer, 10th Edition, McGraw-Hill, New York, 2010.
[38] J.D. Knudsen, D.L. Katz, Fluid Dynamics and Heat Transfer., McGraw-Hill, New York, 1958.
[39] B. Mikić, Thermal contact conductance; theoretical considerations, Int. J. Heat Mass Transf. 17 (2) (1974) 205–214, doi:10.1016/0017-9310(74)90082-9.
[40] A. Pogačnik, M. Kalin, Parameters influencing the running-in and long-term tribological behaviour of polyamide (PA) against polyacetal (POM) and steel, Wear 290–291 (2012) 140–148, doi:10.1016/j.wear.2012.04.017.
[41] A. Pogačnik, A. Kupec, M. Kalin, Tribological properties of polyamide (PA6) in self-mated contacts and against steel as a stationary and moving body, Wear 378–379 (2017) 17–26, doi:10.1016/j.wear.2017.01.118.
[42] T.J. Hoskins, K.D. Dearn, Y.K. Chen, S.N. Kukureka, The wear of PEEK in rolling-sliding contact-simulation of polymer gear applications, Wear 309 (2014) 35–42, doi:10.1016/j.wear.2013.09.014.